

MCMC Marginalisation Bias and Λ CDM tensions

Eoin Ó Colgáin^a Saeed Pourojaghi^b M. M. Sheikh-Jabbari^{b,c}
Darragh Sherwin^a

^aAtlantic Technological University, Ash Lane, Sligo, Ireland

^bSchool of Physics, Institute for Research in Fundamental Sciences (IPM), P.O.Box 19395-5531, Tehran, Iran

^cThe Abdus Salam ICTP, Strada Costiera 11, I-34014 Trieste, Italy

E-mail: eoin.ocolgain@atu.ie, pourojaghi@ipm.ir, jabbari@theory.ipm.ac.ir,
darragh.sherwin@research.atu.ie

Abstract. Probability distributions become non-Gaussian when the flat Λ CDM model is fitted to redshift binned data in the late Universe. We explain mathematically why this non-Gaussianity arises and confirm that Markov Chain Monte Carlo (MCMC) marginalisation leads to biased inferences in observational Hubble data (OHD). In particular, in high redshift bins we find that χ^2 minima, as identified from both least squares fitting and the MCMC chain, fall outside of the 1σ confidence intervals. We resort to profile distributions to correct this bias. Doing so, we observe that $z \gtrsim 1$ cosmic chronometer (CC) data currently prefers a non-evolving (constant) Hubble parameter over a Planck- Λ CDM cosmology at $\sim 2\sigma$. We confirm that both mock simulations and profile distributions agree on this significance. Moreover, on the assumption that the Planck- Λ CDM cosmological model is correct, using profile distributions we confirm a $> 2\sigma$ discrepancy with Planck- Λ CDM in a combination of CC and baryon acoustic oscillations (BAO) data beyond $z \sim 1.5$ that was noted earlier through comparison of least square fits of observed and mock data.

Contents

1	Introduction	1
2	A bias in MCMC marginalisation	3
2.1	Mathematical Foundations	3
2.2	Cosmic Chronometer (CC) Data	4
2.3	Features in CC Data	5
3	Profile Distributions	8
4	A tension with Planck	12
5	Concluding remarks	14
A	Fisher Matrix	17

1 Introduction

The flat Λ CDM model is the minimal model that fits Cosmic Microwave Background (CMB) data. Remarkably, CMB data from the Planck satellite [1] constrains the Λ CDM model to sub-percent errors, thereby not only providing the strongest constraints, but also a concrete prediction for cosmological probes in the late Universe. The unmitigated success of the Λ CDM model is that CMB, Type Ia supernovae (SN) [2, 3] and baryon acoustic oscillations (BAO) [4] agree on a Λ CDM Universe that is approximately 30% matter. Thus, one key prediction of the Planck- Λ CDM model agrees across early and late Universe cosmological probes. Given this non-trivial agreement, any discrepancies that arise elsewhere constitute challenging puzzles.

Nevertheless, one cannot define any *model* for a dynamical system, especially a complicated system like the Universe, using data from a cosmic snapshot.¹ At best, one has a *prediction* and not a model. In recent years, key predictions of Planck data have been challenged by late Universe determinations of the Hubble constant H_0 [5–9] and the $S_8 := \sigma_8 \sqrt{\Omega_m}/0.3$ parameter [10–14]. Given the diversity of the late Universe probes (see reviews [15, 16]), it is highly unlikely that any single systematic can be found to explain the discrepancies. That being said, in astrophysics one can never preclude systematics; 3 decades after Phillips’ seminal paper [17], we are still debating an ad hoc correction for the mass of the host galaxy in Type Ia SN [18–21]. Bearing in mind that Type Ia SN are one of our best understood cosmological probes, one quickly understands that any systematics debate may be endless.

Thus, it is far more expedient to assume that the Λ CDM model is breaking down and to look for tell-tale signatures of model breakdown. If signatures cannot be found, one arrives at a contradiction, and revisits the assumption that the model is breaking down. For physicists, *model breakdown comes about when model fitting parameters return discrepant values at different time slices or epochs*. Translated into astronomy, this equates to discrepant cosmological parameters in different redshift ranges. The usual H_0, S_8 tensions may also be viewed in the same light: a discrepancy between high and low redshift inferences/measurements of

¹Here, we mean CMB data with an effective redshift $z \sim 1100$.

the parameters [15, 16]. Nevertheless, early and late Universe observables are typically not the same, so one is confronted with a rich set of potential systematics.

Within the context of Λ CDM tensions, it was recently observed that the integration constant from the Friedmann equations, aka the Hubble constant H_0 , picks up redshift dependence whenever our model assumption - required to close the Friedmann equations - disagrees with the Hubble parameter $H(z)$ extracted from observations [22, 23]. Similarly, $\rho_{m0} = H_0^2 \Omega_m$, an integration constant of the matter continuity equation, implies matter density Ω_m is a mathematically constant quantity. These are irrefutable predictions from mathematics, i. e. a prediction that is *robust to systematics*. However, observationally H_0 and Ω_m are model fitting parameters and nothing precludes them picking up redshift dependence (except of course if one assumes they do not!), and providing a signature of model breakdown. If this happens in the late Universe within the Λ CDM model, H_0 is correlated with matter density Ω_m , while Ω_m is correlated with $S_8 \propto \sigma_8 \sqrt{\Omega_m}$. Thus, there is at least one simple scenario, namely redshift evolution of cosmological parameters in the late Universe, where “ H_0 tension” and “ S_8 tension” are not independent and simply symptoms of Λ CDM model breakdown.

The next relevant question is, where is the evidence for evolving cosmological parameters in the late Universe? Starting with strong lensing time delay [24, 25],² descending trends of H_0 with redshift have been reported in Type Ia SN [28–33] and combinations of data sets [34, 35]. On the other hand, larger values of Ω_m have been noted in high redshift observables, primarily quasars (QSOs) [36–43],³ but also Type Ia SN [29–31, 45] (see also [46, 47]). Note, as emphasised earlier, if H_0 evolves at the background level, correlated fitting parameters are expected to also evolve. Moreover, mock analysis within the Λ CDM setting reveals that evolution of best fit (H_0, Ω_m) parameters cannot be precluded, and conversely possesses a finite likelihood, in either observational Hubble data (OHD) *or* angular diameter distance data *or* luminosity distance data [48]. We stress that this result *rests on mock analysis*; it represents a purely mathematical statement about the Λ CDM model that is independent of systematics.

Separately, at the perturbative level, redshift evolution of S_8 or σ_8 has been reported in galaxy cluster number counts and Lyman- α spectra [49], $f\sigma_8$ constraints from peculiar velocities and redshift space distortions (RSD) [50], comparison between weak [10–12] and CMB lensing [51, 52]. What is important here is that these observations appear to restrict the evolution in S_8 to the late Universe. In [53] the possibility was raised that “*tracers at higher redshift and probing larger scales prefer higher S_8* ”.⁴ Nevertheless, one can argue against evolution with scale on the grounds that cosmic shear [10–12], which is sensitive to smaller scales (larger k), and peculiar velocity constraints [13, 14], which are sensitive to larger scales (smaller k), both prefer lower values of S_8 . Moreover, both galaxy clusters and Lyman- α spectra are expected to probe similar scales.⁵ Thus, if systematics are not impacting results, then redshift evolution is the only point of agreement in the observations [10–12, 49–53].

²Systematics are explored in [25] and the descending trend is not an obvious systematic. The lensed system RXJ1131-1231 [26], which partly drives the trend, has recently been re-analysed using spatially resolved stellar kinematics of the host galaxy [27], and the higher H_0 value remains robust, admittedly with inflated errors. As TDCOSMO project to analyse 40 lenses, the prospect of a discovery of a descending H_0 trend assuming the Λ CDM model remain strong.

³Just as with Type Ia SN, the systematics of QSOs are being investigated [44].

⁴There are also conflicting observations of high redshift σ_8 or S_8 values that are lower than Planck in the late Universe [54, 55], so either this trend is not universal, or systematics are at play.

⁵We thank Matteo Viel for correspondence on this point.

Note also that redshift is more fundamental than scale in FLRW cosmology; one must solve the Friedmann equations in either time or redshift before one contemplates any discussion of scale.

The purpose of this letter is to revisit the analysis presented in [30, 48], where the evidence for evolution was quantified on the basis of mock simulations and not Markov Chain Monte Carlo (MCMC), the technique most familiar in cosmology. The fundamental problem is that once one bins low redshift data and studies evolution of cosmological parameters with bin redshift, one quickly encounters projection effects in MCMC analyses. These effects are not just the preserve of exotic models [56–58], such as Early Dark Energy (EDE) [59, 60], and happen in the simplest model when one bins data. The most striking demonstration of the resulting bias is that the peaks of MCMC posteriors no longer coincide with the minimum of the likelihood (see [57]). Ultimately, this bias is expected because one is working in a regime of the Λ CDM model with non-Gaussian probability distributions [48] (see also [30]).

The structure of this paper is as follows. In section 2 we confirm the bias in MCMC marginalisation. In section 3 we introduce profile distributions (PDs) [57] as a means of addressing the bias and confirm that the statistical significance of discrepancies from mock simulations agree well with PD analysis. In section 4, we revisit and confirm the high redshift OHD tensions reported in [30]. We end in section 5 with concluding remarks.

2 A bias in MCMC marginalisation

In this section we illustrate a bias in MCMC marginalisation that arises in the (flat) Λ CDM model when data is binned by redshift. This bias can be traced to a regime of the Λ CDM model with non-Gaussian distributions and is independent of systematics [30, 48].

2.1 Mathematical Foundations

Consider an exercise where one bins OHD and confronts it to the Λ CDM Hubble Parameter $H(z)$ in the late Universe, a setting where the radiation sector can be safely decoupled. In high redshift bins ($z \gg 0$) in the matter-dominated regime, the Hubble parameter becomes insensitive to the dark energy (DE) sector:

$$H(z) = H_0 \sqrt{1 - \Omega_m + \Omega_m(1+z)^3} \xrightarrow{z \gg 0} H_0 \sqrt{\Omega_m} (1+z)^{\frac{3}{2}}. \quad (2.1)$$

More concretely, taking $z \rightarrow \infty$ we see that data can only constrain the combination $\rho_{m0} = H_0^2 \Omega_m$. For *hypothetical* data in a redshift bin with effective redshift $z = \infty$, this means that one can only constrain the combination $\Omega_m h^2$ ($h := H_0/100$), but H_0 and Ω_m remain unconstrained. Alternatively put, for any given $\Omega_m h^2$ constraint, there is an infinite number of corresponding (H_0, Ω_m) pairs. Translated into a probability density function (PDF), this is simply the statement that in a very high redshift bin at $z = \infty$, one expects uniform or flat distributions for H_0 and Ω_m with the model (2.1).

Of course, observed data resides at finite z and not $z = \infty$. As a result, one does not encounter *exactly* flat PDFs in H_0 and Ω_m at high redshift, but *almost* flat PDFs. More important to us is the observation that these PDFs must flatten in a non-Gaussian manner. To appreciate this fact, we observe that high redshift OHD only constrains $\Omega_m h^2$ well.⁶ For this

⁶Note that observables like SN or QSO that measure $D_L(z) = c(1+z) \int_0^z dz'/H(z')$ are mainly sensitive to the low redshift part of $H(z)$, i. e. the combination $H_0^2(1 - \Omega_m)$, and in this sense they are complementary to the OHD data which is more sensitive to high redshift part of $H(z)$, $H_0^2 \Omega_m$. The complementarity can

reason, best fit parameters are constrained to a $\Omega_m h^2 = \text{constant}$ curve in the (H_0, Ω_m) -plane. The almost flat H_0 and Ω_m PDFs can only arise if this curve stretches in the (H_0, Ω_m) -plane. As a result of this stretching, one ends up with a relatively uniform distribution on a curve. At the extremes of the curve, one finds a distribution of large H_0 values, which do not differ greatly in Ω_m , and they get projected to a peak at small values on the Ω_m axis. Conversely, at the other end of the curve, one finds a distribution of small Ω_m values, which do not differ greatly in H_0 , and they get projected onto a peak at large values on the H_0 axis. This is a “projection effect” in common cosmology parlance. It is driven by the irrelevance of the DE sector at high redshift and the constraint $\Omega_m h^2 = \text{constant}$ from the Λ CDM model (2.1). Together these features distort the distribution away from a Gaussian configuration.

Thus, simply by binning and fitting OHD to the Λ CDM model one enters a non-Gaussian regime as the effective redshift of the bin increases. This effect, which is expected from the purely mathematical arguments above, has been confirmed in mock data [30, 48], and in line with expectations, we demonstrate that it impacts MCMC inferences with observed data in the next subsection.

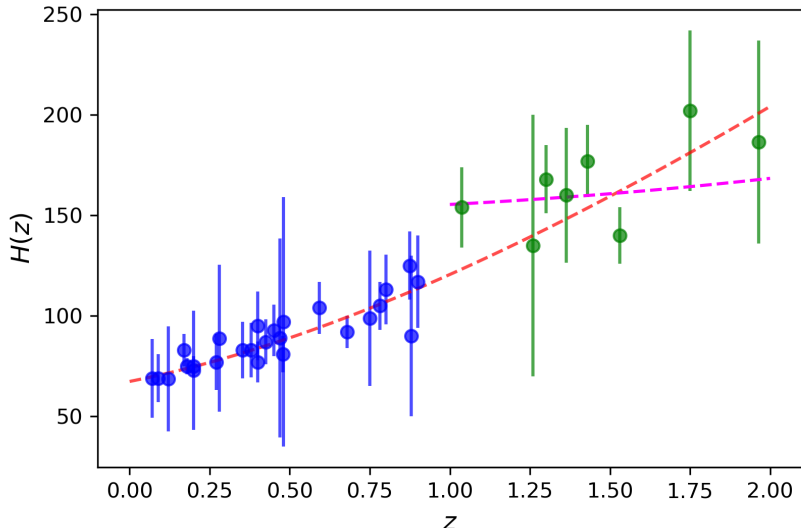


Figure 1. The CC data split above and below $z = 1$ alongside the Planck- Λ CDM $H(z)$ (dashed red) and best fit $H(z)$ (dashed magenta) above $z = 1$. From the high redshift data (green), it is evident that a horizontal $H(z)$ correspond to $\Omega_m = 0$ is preferred.

2.2 Cosmic Chronometer (CC) Data

Here we work with OHD from the cosmic chronometer (CC) program [61]. Concretely, we work with 34 $H(z)$ constraints spanning the redshift range $0.07 \leq z \leq 1.965$ [62–69]. We illustrate the data in Fig. 1, where it is consistent with Fig. 9 of [69] modulo the fact that we have an additional data point at $z = 0.8$, which is not independent. See Table 1.1 of [70]. While CC data may eventually be good enough to arbitrate on Hubble tension [70], the data is not good enough on its own to do cosmology. To put this comment in context,

be demonstrated by combining $H(z)$ and $D_L(z)$ constraints and checking that one recovers mock data input parameters in all redshift bins [48].

we observe that the errors in Fig. 1 do not include systematic errors (see [71] for an account of the systematics). As a result the constraints we get on cosmological parameters will be underestimated. Thus, from our perspective the data in Fig. 1 is simply some representative cosmological data in the OHD class.

Methodology: We impose a low redshift cut-off on the OHD z_{\min} , removing all data points with redshifts $z_i < z_{\min}$, and then extremising the χ^2 likelihood,

$$\chi^2 = Q^T \cdot C^{-1} \cdot Q, \quad (2.2)$$

where C is the covariance matrix, which is simply the square of the H_i errors on the diagonal, and Q is the vector,

$$Q_i = H_i - H_{\text{model}}(z_i), \quad (2.3)$$

where $H_i := H(z_i)$ denotes OHD and $H_{\text{model}}(z)$ is the model (2.1) without the high redshift limit. The best fit (H_0, Ω_m) parameters correspond to the minimum of the χ^2 , while on the assumption of Gaussian errors, we estimate the errors from a Fisher matrix (appendix A). In parallel, we perform MCMC marginalisation through *emcee* [72]. More concretely, subject to the priors $H_0 \in [0, 200]$ and $\Omega_m \in [0, 1]$, the latter restricting us to a physical regime, we record 16th, 50th and 84th percentiles for MCMC posteriors, as is common practice with Gaussian distributions. Thus, both techniques are tailored to Gaussian posteriors, yet non-Gaussianities will be evident in MCMC posteriors. By comparing the output from these two techniques in Table 1 for different values of z_{\min} we observe that error estimates from Fisher matrix and MCMC quickly disagree as z_{\min} increases.

From Table 1, we see that MCMC inferences lead to non-Gaussian 1σ confidence intervals, where in line with the expectations from [48], H_0 errors are larger for smaller values, and Ω_m errors are larger for larger values, respectively. This is expected if the H_0 and Ω_m posteriors are peaked at larger and smaller values, respectively, in line with our earlier mathematical argument. Only for the full data set with $z_{\min} = 0$ do we find reasonable agreement between the Fisher matrix and MCMC 1σ confidence intervals. As can be seen from the lopsided MCMC confidence intervals, the non-Gaussianity becomes more pronounced with increasing z_{\min} . Interestingly, beyond $z_{\min} = 1$, the minimum of the χ^2 falls outside of the MCMC 1σ confidence intervals. Nevertheless, by evaluating the MCMC chains on the χ^2 likelihood (2.2), we confirm that the parameters corresponding to the minimum χ^2 value are tracking the best fit. Note, the peak of the MCMC posterior is no longer a measure of goodness of fit and inferences have become biased in a regime of model parameter space where distributions are expected to be inherently non-Gaussian. Our analysis here underscores potential problems with a blind MCMC analysis with the traditional 16th, 50th and 84th percentiles.

2.3 Features in CC Data

Once one accounts for biases, it is clear from Table 1 that there are trends in CC data when it is binned. Starting from $z_{\min} = 0$ through to $z_{\min} = 0.6$ we see a decreasing trend in best fit values of H_0 (also central H_0 values from MCMC), which is compensated by an increasing trend in Ω_m best fit values. From Fig. 1 it is difficult to visibly discern any trend from the raw data. From $z_{\min} = 0.7$ through to $z_{\min} = 1.4$, there is in contrast a preference for larger H_0 and smaller Ω_m values. This trend is evident from the raw data, where at higher redshifts one sees large scatter and large fractional errors in the data. For $z_{\min} = 1$, it is clear that the best fit line in magenta corresponding to $(H_0, \Omega_m) = (150.4, 0.01)$ (Table 1) is closer to

z_{\min}	# CC	Fisher Matrix		MCMC	
		H_0 (km/s/Mpc)	Ω_m	H_0 (km/s/Mpc)	Ω_m
0	34	68.14 ± 3.07	0.320 ± 0.059	$67.76^{+3.03}_{-3.09}$ (68.12)	$0.328^{+0.065}_{-0.055}$ (0.321)
0.2	27	65.03 ± 6.65	0.368 ± 0.118	$63.05^{+6.64}_{-7.23}$ (64.98)	$0.405^{+0.170}_{-0.111}$ (0.369)
0.4	22	62.42 ± 8.38	0.411 ± 0.161	$59.54^{+8.30}_{-8.22}$ (62.39)	$0.470^{+0.229}_{-0.151}$ (0.411)
0.6	15	59.83 ± 17.21	0.454 ± 0.338	$56.45^{+13.16}_{-9.33}$ (59.86)	$0.526^{+0.288}_{-0.225}$ (0.453)
0.7	14	79.11 ± 19.40	0.222 ± 0.162	$67.59^{+19.19}_{-16.57}$ (79.18)	$0.344^{+0.344}_{-0.178}$ (0.222)
0.8	11	103.97 ± 24.94	0.097 ± 0.088	$82.43^{+28.33}_{-27.03}$ (104.02)	$0.206^{+0.357}_{-0.131}$ (0.096)
1	8	150.37 ± 31.21	0.010 ± 0.035	$108.92^{+33.94}_{-44.47}$ (150.38)	$0.087^{+0.304}_{-0.068}$ (0.010)
1.2	7	154.35 ± 42.95	0.006 ± 0.042	$83.07^{+48.52}_{-32.19}$ (154.47)	$0.194^{+0.439}_{-0.159}$ (0.006)
1.4	4	125.41 ± 79.55	0.039 ± 0.132	$65.32^{+44.88}_{-20.30}$ (125.44)	$0.320^{+0.423}_{-0.250}$ (0.039)
1.5	3	36.12 ± 72.69	1.000 ± 4.269	$55.19^{+34.64}_{-14.73}$ (36.16)	$0.393^{+0.387}_{-0.283}$ (0.999)

Table 1. Comparison between Fisher matrix and MCMC analysis for CC data with a low redshift cut-off z_{\min} . We record the number of data points, the extremum of the χ^2 and 1σ confidence interval estimated from the Fisher matrix, 16th, 50th and 84th percentiles from MCMC posteriors corresponding to 1σ confidence intervals, and the minimum χ^2 from the MCMC chain in brackets. MCMC marginalisation exhibits non-Gaussian 1σ confidence intervals, and for $z_{\min} > 1$, the minimum value of the χ^2 from the MCMC chain falls outside of this interval. The latter tracks the best fit up to small numbers in line with expectations.

horizontal line than the Planck- Λ CDM cosmology in red. To be more explicit, for $z_{\min} = 0$, $\rho_{m0} := H_0^2 \Omega_m \simeq 1500$ which is close to the Planck value, whereas for $z_{\min} = 1$, $\rho_{m0} \simeq 225$. The sharp drop in ρ_{m0} means the magenta line should be almost horizontal. For $z_{\min} = 1.5$, we switch to an opposite regime of parameter space with unexpectedly low and high values of H_0 and Ω_m , respectively, a trend which is evident in the data, but there are only three data points. Despite, the small number of data points, the tendency for smaller H_0 and larger Ω_m inferences within Λ CDM cosmology at high redshifts has been documented across three independent observables [30]. We will come back to this claim in section 4. Finally, it is worth noting that for large z_{\min} and samples with few data points, one expects broad MCMC posteriors. These posteriors are severely impacted by the prior on Ω_m , as is evident from Table 1.

For the moment we leave physical speculations to the discussion and return to the trend in CC data above $z = 1$ favouring less evolution in the Hubble parameter than the Planck- Λ CDM model. We would like to quantify the significance of this trend, but since we are working in a non-Gaussian regime of the model, we can expect both Fisher matrix and MCMC to give biased results. In Fig. 2 we show MCMC posteriors for $z > 1$ CC data in blue alongside posteriors for low redshift ($z < 1$) CC data, which is simply added to aid comparison and also highlight the Gaussianity of the low redshift posteriors. One notes that the peaks of the $z > 1$ distributions are a little displaced from to the values minimising the χ^2 . However, the emergence of the lower peak in the H_0 posterior at $H_0 \sim 50$ km/s/Mpc has the hallmarks of a projection effect. To appreciate this, note that the configurations in the blue curve in the top left corner of the 2D posterior are projected onto the lower H_0 peak.

Moreover, if one shifts the H_0 peak from $H_0 \sim 150$ to $H_0 \sim 50$ km/s/Mpc while maintaining $\Omega_m \sim 0$, this shifts the magenta curve in Fig. 1 outside of all the data points, so the lower H_0 peak is a phantom artefact unrelated to the goodness of fit. We also observe a shift in the higher H_0 peak away from the minimum of the χ^2 .

Ignoring these features, one could attempt to interpret the overlap in the 2D posteriors in Fig. 2. Doing so, one may conclude that low and high redshift CC data are consistent within 1σ . However, since Hubble tension is a 1D problem (local H_0 determinations are insensitive to other parameters), to compare with locally observed values of H_0 one needs to project onto the H_0 axis. Alternatively put, Hubble tension is a problem in 1D posteriors. Projecting onto the H_0 axis by determining 16th, 50th and 84th percentiles, one sees from Table 1 that the $z_{\min} = 1$ MCMC confidence interval encloses the $z_{\min} = 0$ central values within 1σ ,⁷ but not the point in parameter space that best fits the data!

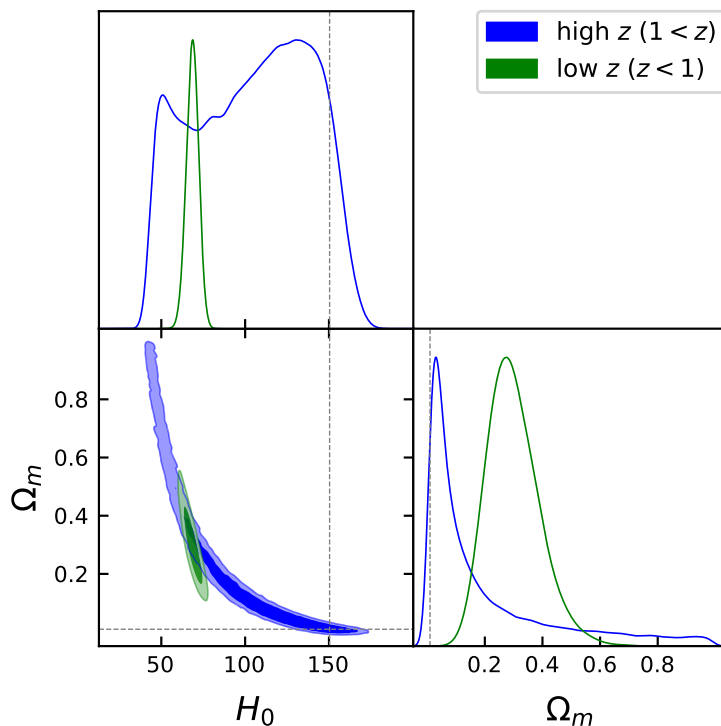


Figure 2. Cosmological parameter inferences from MCMC chains for the CC data split at $z = 1$. Dashed lines denote the extremum of the χ^2 . For high redshift data, Ω_m is consistent with $\Omega_m = 0$, implying a constant Hubble parameter $H(z) = \text{constant} \sim 150$ km/s/Mpc. The secondary peak evident in the H_0 posterior arises from projecting the long tails in the Ω_m posterior onto the H_0 axis. The dashed lines correspond to the best fit parameters of the high z sample $(H_0, \Omega_m) = (150.37, 0.0098)$. This agrees well with the minimum χ^2 from the MCMC chain, $(H_0, \Omega_m) = (150.27, 0.0099)$.

Evidently, given the non-Gaussian posteriors, care is required when interpreting the significance of the trend towards a non-evolving (horizontal) $H(z)$ at higher redshifts in Fig. 1. We cannot use the errors from the Fisher matrix as we are clearly in a non-Gaussian regime, whereas MCMC inferences are impacted by projection effects to the extent that the minimum

⁷Note, removing the eight high redshift data points from the $z_{\min} = 0$ sample will not shift the central values much.

of the χ^2 (confirmed from the MCMC chain) falls outside of the 1σ confidence interval. For this reason, we resort to mock simulations. While this may seem a little redundant if we are going to employ profile distributions in section 3, there is motivation for this exercise. In [30] the significance of a descending H_0 /increasing Ω_m trend with effective redshift in OHD, Type Ia SN and QSOs was estimated to be a $\sim 3\sigma$ effect on the basis of combining $\sim 2\sigma$ effects in each of the *independent* data sets using Fisher’s method. Here, working with the same data throughout, we can directly compare the significance of a discrepancy estimated through mock simulations from the significance of a discrepancy estimated through profile distributions. In particular, we will address the question: how significant is a constant $H(z)$ with $z_{\min} = 1$ (8 data points) against the Planck consistent cosmology favoured by the full data set ($z_{\min} = 0$ entry in Table 1)? Note, the significance will be overestimated due to missing systematic uncertainties (see [71]), but we can still make comparison between the two techniques.

Mock simulations: To address this question using mock simulations, we begin with the MCMC chains for the full sample. For each entry in the MCMC chain (approximately 15,000 entries in total), we generate a new realisation of the 8 high redshift data points ($z > 1$) that are by construction statistically consistent with both the best fits from the full sample and also the Planck- Λ CDM values [1]. More concretely, for each (H_0, Ω_m) entry in our MCMC chain, we displace the data points to the corresponding Λ CDM Hubble parameter before generating new data points in a normal distribution where the errors serve as standard deviations. We then fit back the Λ CDM model to each realisation of the mock data and record the best fit (H_0, Ω_m) values, which give us a distribution of expected (H_0, Ω_m) best fits. The distributions are presented in Fig. 3 alongside the best fits from observed data. Throughout, we assume canonical values $(H_0, \Omega_m) = (70, 0.3)$ for the initial guess of the fitting algorithm. Best fits can saturate our bounds, i. e. $\Omega_m = 0$ and $\Omega_m = 1$, and this leads to an unsightly pile up of best fits at $\Omega_m = 0$ and $\Omega_m = 1$ in Fig. 3 [30]. It is important to retain all the configurations, otherwise one is not accounting for the probability that a best fit falls outside our priors. As a consistency check, we see that the median or 50th percentile, $(H_0, \Omega_m) = (68.32, 0.321)$ agrees well with the mock input parameters, thereby demonstrating that there are an equal number of best fits with values above and below the injected parameters in the mocks. We find that probability of a more extreme (larger) H_0 value to be $p = 0.022$, while the probability of a more extreme (smaller) Ω_m value to be $p = 0.035$, respectively. Converted into a Gaussian statistic, these correspond to 2σ and 1.8σ , respectively, for a one-sided normal distribution. Thus, on the basis of mock simulations, we estimate the non-evolving constant $H(z)$ with $z_{\min} = 1$ as a $\sim 2\sigma$ effect. In the next section we will recover this number more or less from the profile distribution analysis.

3 Profile Distributions

Having explained the mathematics behind the bias, which gives rise to a projection effect, in subsection 2.1, and having illustrated how it affects MCMC inferences in subsection 2.2 - the minimum of the χ^2 may fall outside of 1σ confidence intervals - we turn to profile distributions (PDs) [57], an extension of the profile likelihood, e. g. [76], in order to address the bias. Consider two sets of parameters θ_1 and θ_2 and a normalised distribution $\mathcal{P}(\theta_1, \theta_2)$.

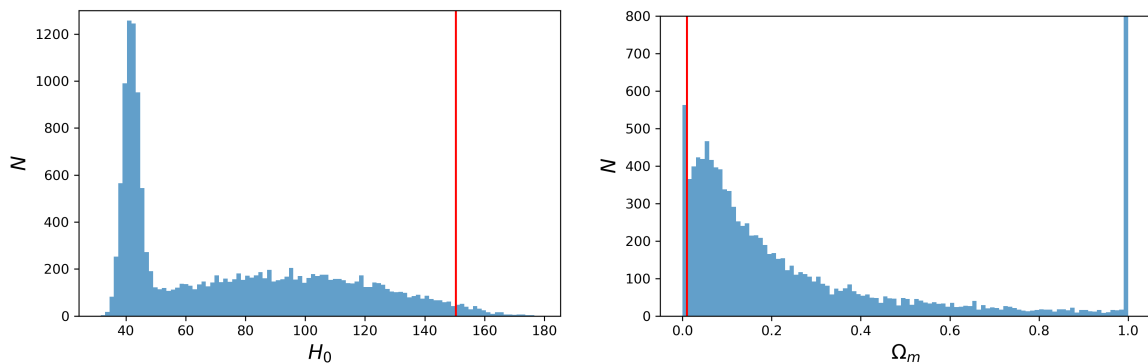


Figure 3. PDFs of best fit parameters from mock CC data with $z_{\min} = 1$ (8 data points). The injected (H_0, Ω_m) parameters come from the MCMC chain for the full sample ($z_{\min} = 0$ entry in Table 1). The best fits from observed data are denoted by solid red lines. Numerous best fits saturate our bounds both at $\Omega_m = 0$ and $\Omega_m = 1$ leading to an unusual peak in the H_0 PDF at $H_0 \sim 40$ km/s/Mpc. Removing this feature, it is evident that the H_0 peak and Ω_m peak have been shifted to larger and smaller values, respectively, in line with expectations from a projection effect. There is a low probability ($p = 0.022$ for H_0 , $p = 0.035$ for Ω_m) of finding larger H_0 and smaller Ω_m than observed best fits (red lines) from the mock best fits.

The basic idea [57] is to study the ratio

$$R(\theta_1) = \frac{\tilde{\mathcal{P}}(\theta_1)}{\max_{\theta_1} \tilde{\mathcal{P}}(\theta_1)} = \frac{\tilde{\mathcal{P}}(\theta_1)}{\max_{\theta_1, \theta_2} \mathcal{P}(\theta_1, \theta_2)}, \quad (3.1)$$

where $\tilde{\mathcal{P}}(\theta_1)$ is the PD, defined to be the maximum of \mathcal{P} for each θ_1 along the θ_2 direction:

$$\tilde{\mathcal{P}}(\theta_1) = \max_{\theta_2} \mathcal{P}(\theta_1, \theta_2). \quad (3.2)$$

The advantage of this approach is that $R(\theta_1)$ can serve as a probability distribution function (up to an overall normalization), however we do not need to perform any integration, so $R(\theta_1)$ is not prone to volume or projection effects. At this juncture, given the simplicity of our setup with only two parameters (H_0, Ω_m) , we can be more explicit. Consider the probability distribution,

$$\mathcal{P}(\theta_1, \theta_2) = \exp\left(-\frac{1}{2}\chi^2(\theta_1, \theta_2)\right), \quad (3.3)$$

where $\theta_i \in \{H_0, \Omega_m\}$ and $\chi^2(H_0, \Omega_m)$ is our earlier likelihood (2.2). The maximum value of \mathcal{P} occurs for the minimum value of χ^2 from the MCMC chain, $\mathcal{P}_{\max} = e^{-\frac{1}{2}\chi_{\min}^2}$. In this concrete setting, the PD becomes

$$\tilde{\mathcal{P}}(\theta_1) = e^{-\frac{1}{2}\chi_{\min}^2(\theta_1)}, \quad (3.4)$$

where $\chi_{\min}^2(\theta_1)$ denotes the minimum value of the χ^2 along the θ_2 direction for a fixed θ_1 value. It should not be confused with the overall minimum χ_{\min}^2 , which can be extracted easily from the MCMC chain. In practice, one can also determine $\chi_{\min}^2(\theta_1)$ from the MCMC chain by breaking the θ_1 direction up into bins and finding the minimum of the χ^2 for each bin. Having done so, we are in a position to define a PDF [57]:

$$w(\theta_1) = \frac{e^{-\frac{1}{2}\chi_{\min}^2(\theta_1)}}{\int e^{-\frac{1}{2}\chi_{\min}^2(\theta_1)} d\theta_1} = \frac{R(\theta_1)}{\int R(\theta_1) d\theta_1}, \quad (3.5)$$

where in the second equality we have divided top and bottom by $\mathcal{P}_{\max} = e^{-\frac{1}{2}\chi_{\min}^2}$. As a result, $R(\theta_1) = e^{-\frac{1}{2}\Delta\chi_{\min}^2}$, where $\Delta\chi_{\min}^2 := \chi_{\min}^2(\theta_1) - \chi_{\min}^2$, so that $R(\theta_1)$ peaks at $R(\theta_1) = 1$. Note that $\int_{-\infty}^{+\infty} w(\theta_1) d\theta_1 = 1$ by construction, so $w(\theta_1)$ describes a properly normalised PDF. Thus we can identify the 1σ , 2σ and 3σ confidence intervals corresponding to the 68%, 95% and 99.7% confidence level, respectively, by simply identifying $\theta_1^{(1)}$ and $\theta_1^{(2)}$ such that [57]

$$\int_{\theta_1^{(1)}}^{\theta_1^{(2)}} w(\theta_1) d\theta_1 = I, \quad w(\theta_1) = w(\theta_2), \quad I \in \{0.68, 0.95, 0.997\}. \quad (3.6)$$

We will outline how these conditions can most easily be satisfied when we turn to explicit examples.

Our first port of call is making sure that the PD methodology gives sensible results. This can be best judged by applying it to the CC data with $z_{\min} = 0$, since this is where we expect a distribution closest to a Gaussian distribution, as is evident from the agreement between Fisher matrix and MCMC results in Table 1. In particular, we will be interested in a comparison between 1σ confidence intervals to make sure that (3.6) is not underestimating or overestimating the 1σ confidence interval.

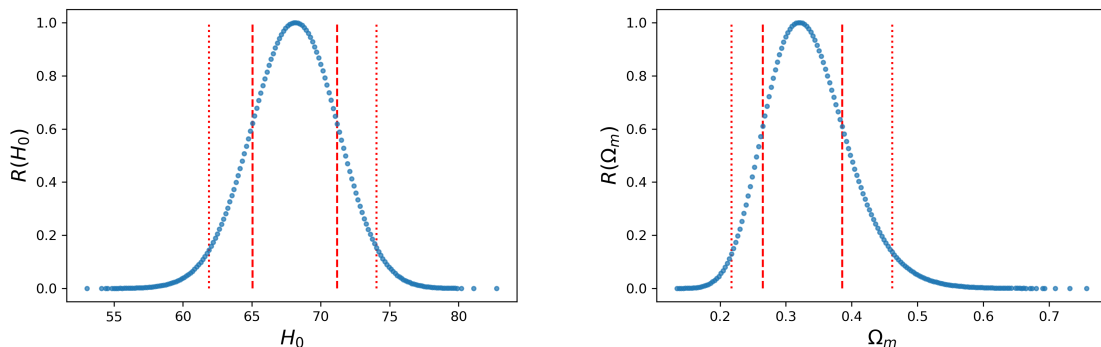


Figure 4. $R(H_0)$ and $R(\Omega_m)$ distributions for the full CC data set ($z_{\min} = 0$) in Fig. 1. The dashed and dotted lines denote 1σ and 2σ confidence intervals.

We start by running a long MCMC chain (100,000 iterations) in order to ensure bins are well populated, and begin by analysing $\theta_1 = H_0$ with $\theta_2 = \Omega_m$. From the MCMC chain we identify the smallest and largest value of H_0 in the chain and break up this range into approximately 200 uniform bins, which we label using the H_0 value at the centre of the bin. We omit any empty bins. One can increase the number of bins by simply running a longer MCMC chain. In each H_0 bin we identify the minimum value of the χ^2 , $\chi_{\min}^2(H_0)$, and calculate $R(H_0)$. One then repeats the steps for Ω_m . In Fig. 4 we plot $R(H_0)$ against H_0 and $R(\Omega_m)$ against Ω_m , noting that the distributions are Gaussian to first approximation.

Since the distributions from the MCMC chain are sparse in the tails, empty bins are evident in Fig. 4. Nevertheless, with 200 bins, modulo any empty bins, we have sufficient density of points to calculate the total area under the $R(H_0)$ and $R(\Omega_m)$ curve using Simpson's rule. Any concern about precision can simply be mitigated by running a longer MCMC chain and increasing the number of bins. One may directly use $R(H_0) \leq 1$ and $R(\Omega_m) \leq 1$ to find 68, 95 and 99.7 percentiles, respectively corresponding to 1σ , 2σ and 3σ confidence intervals. Consider $F_\kappa := \int_{R \geq \kappa} R(\theta_1) d\theta_1$, where $\kappa \leq 1$. Observe that $F_{\kappa=1} = 0$ and $F_{\kappa=0} := F_0 =$

$\int R(\theta_1)d\theta_1$. Then move κ through and terminate the process when F_κ/F_0 is equal to 0.68, 0.95 and 0.997. This gives the corresponding range for θ_1 that defines the confidence interval. Working with the precision afforded to us by approximately 200 bins, the H_0 and Ω_m 1σ confidence intervals are presented in Fig. 4 and the first entry in Table 2. The outcome is in excellent agreement with both Fisher matrix and MCMC analysis. In particular, a mild non-Gaussianity in Ω_m is evident in both Fig. 4 and the errors. Thus, we have succeeded in recovering results in the (almost) Gaussian regime that are consistent with Fisher matrix and MCMC analysis and this provides an important check of the methodology.

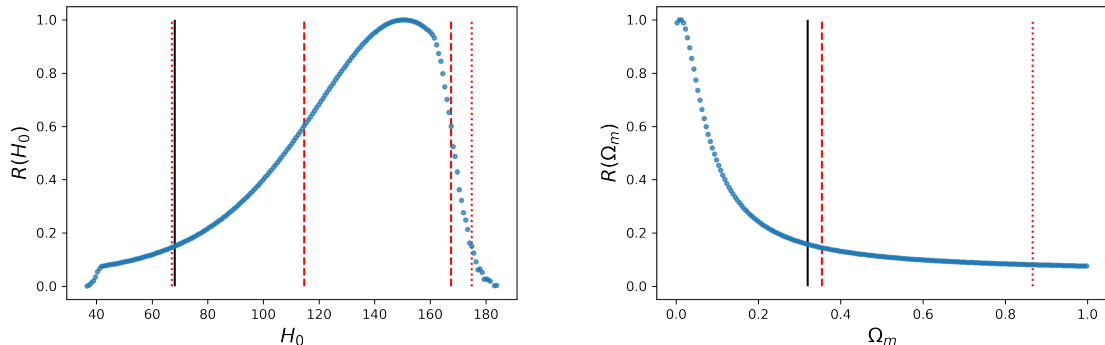


Figure 5. Same as Fig. 4 but a truncated CC data set of 8 high redshift data points with $z_{\min} = 1$. The black lines denote the best fit values from the full sample, $(H_0, \Omega_m) = (68.2, 0.320)$.

We now apply the same PD methodology to the non-Gaussian regime where MCMC marginalisation leads to biased results. To be concrete, we focus on the eight data points in the range $1 < z < 2$ where a non-evolving $H(z)$ trend is evident in the raw data in Fig. 1. Our goal here is to quantify the disagreement with the full data set, where one infers $H_0 \sim 68$ km/s/Mpc and $\Omega_m \sim 0.32$. A similar exercise was performed in subsection 2.3 with mock simulations and the disagreement was estimated to be approximately 2σ . Repeating the steps outlined above for the CC data with $z_{\min} = 1$ we find the distributions in Fig. 5. The first observation is that the distributions are non-Gaussian, but a comparison to the MCMC posteriors from the same data in blue in Fig. 2 reveals that there is no secondary H_0 peak at $H_0 \sim 50$ km/s/Mpc. Thus, we confirm the secondary peak to be a projection effect. That being said, the primary H_0 peak from Fig. 2 has shifted to the dashed line corresponding to the minimum of the χ^2 , since the peak of the distribution and χ^2 minimum agree by construction. Comparing the blue Ω_m distribution from Fig. 2 to the $R(\Omega_m)$ distribution in Fig. 5, we see that the peak is close to $\Omega_m = 0$ and that the tails continue to $\Omega_m = 1$. In both plots we see that there is a non-zero probability of inferring $\Omega_m = 1$. In some sense, this is not so surprising, the reason being that one is free to adopt generous priors for H_0 , so that probability of large and small H_0 values is zero, but the priors on Ω_m in the flat Λ CDM model are restricted. For this reason, as a distribution spreads one invariably finds that distributions are impacted by the Ω_m priors.⁸

It is evident from Fig. 5 that any tension that exists is confined to the H_0 parameter. Moreover, since there may be only one binned value of Ω_m below the $R(\Omega_m)$ peak, at the

⁸Note, this is a problem for the flat Λ CDM model. In particular, one may easily find that the peak of the Ω_m distribution is larger than $\Omega_m = 1$, as is the case with Hubble Space Telescope SN with redshifts $z > 1$ in the Pantheon+ sample [31].

precision afforded to us by 200 bins, the $R(\Omega_m)$ distribution in Fig. 5 is essentially one-sided and the 1σ confidence interval stretches beyond $\Omega_m \sim 0.32$, so there is no disagreement in the Ω_m parameter. Nevertheless, in the H_0 parameter we see that $H_0 \sim 68$ km/s/Mpc, the value favoured by the full data set is just under 2σ removed from the peak. The main point here is that, as is obvious from the raw data, current CC data with $z > 1$ has a preference for a non-evolving Hubble parameter $H(z)$ with a large constant $H_0 \sim 150$ km/s/Mpc. The disagreement is just under 2σ , more accurately 1.9σ from $R(H_0)$, and only 0.9σ from $R(\Omega_m)$. Although this may not be a serious discrepancy, essentially because of the poor data quality (8 data points), this disagreement supports the $\sim 2\sigma$ discrepancy seen in the mock simulations. It should be borne in mind that systematic uncertainties have been omitted and these will reduce this discrepancy once properly propagated. Given the agreement between the PD and mock simulation analysis, there is nothing to suggest that the three independent trends highlighted in [30] across OHD, Type Ia SN and QSOs are not *bona fide* disagreements and that redshift evolution is present in the sample. The task remains to combine them at the level of a χ^2 likelihood instead of combining them using Fisher’s method on the basis that they are independent probabilities. We leave this exercise for a forthcoming paper, but revisit the tension in OHD data in the following section. For completeness, in Table 2 we perform a reanalysis of CC data subsets with the PD approach and record the 1σ intervals.

z_{\min}	# CC	PD	
		H_0 (km/s/Mpc)	Ω_m
0	34	$68.15^{+3.04}_{-3.11}$	$0.320^{+0.065}_{-0.055}$
0.2	27	$65.03^{+6.52}_{-7.03}$	$0.368^{+0.167}_{-0.110}$
0.4	22	$62.42^{+7.78}_{-8.74}$	$0.411^{+0.236}_{-0.113}$
0.6	15	$59.75^{+11.73}_{-13.97}$	$0.455^{+0.355}_{-0.160}$
0.7	14	$79.10^{+16.42}_{-20.56}$	$0.222^{+0.386}_{-0.117}$
0.8	11	$103.94^{+22.88}_{-28.54}$	$0.097^{+0.378}_{-0.074}$
1	8	$150.35^{+17.12}_{-35.95}$	< 0.339
1.2	7	$154.26^{+14.88}_{-54.82}$	< 0.570
1.4	4	$124.81^{+35.38}_{-52.60}$	< 0.661
1.5	3	$36.11^{+72.87}_{-2.43}$	> 0.354

Table 2. Same as Table 1 but with the PD methodology in lieu of Fisher matrix and MCMC analysis. The high redshift $R(\Omega_m)$ distributions are typically one-sided, so one encounters 1σ upper and lower bounds.

4 A tension with Planck

A 2σ ($p = 0.021$) tension with Planck has been reported in OHD through best fits and mock simulations in [30]. In particular, it was noted that a combination of 7 CC and BAO data points above $z = 1.45$ resulted in a $(H_0, \Omega_m) = (37.8, 1)$ best fit, where in line with analysis here, an $\Omega_m \in [0, 1]$ uniform prior was assumed. Based on mock simulations, the probability of such a best fit configuration arising by chance in mocks assuming input parameters consistent

with Planck was estimated to be $p = 0.021$ [30]. A similar best fit appears in the last entry of Table 1 and Table 2, but there is no tension with Planck within the errors, even with our PD analysis, because CC data is inherently of poorer quality than BAO data. One further difference between the analysis is that [30] imposes a Gaussian Planck prior $\Omega_m h^2 = 0.1430 \pm 0.0011$ [1]⁹ to fix the high redshift behaviour of $H(z)$, whereas our analysis here so far has not introduced a prior.

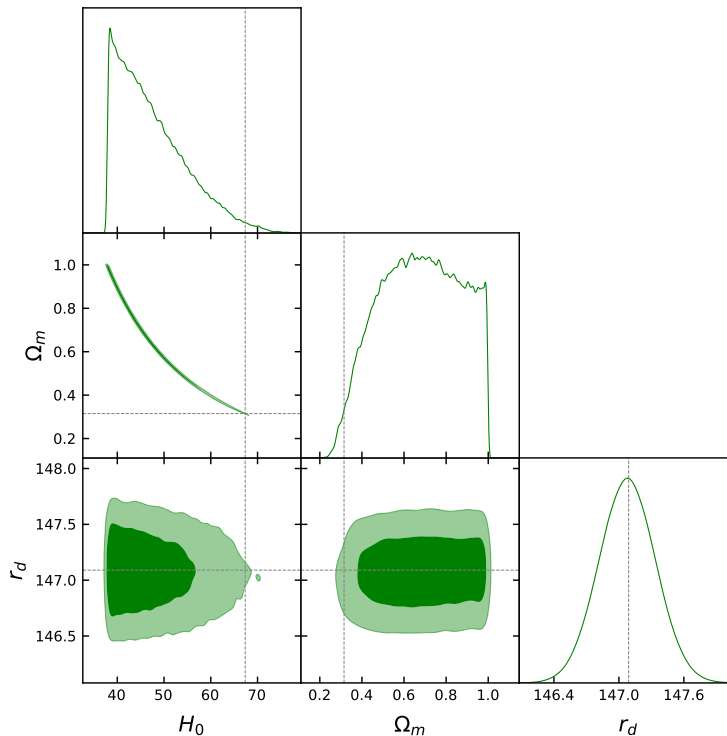


Figure 6. MCMC posteriors for high redshift CC and BAO data subject to Planck priors on $\Omega_m h^2$ and r_d . Dashed lines mark the Planck central values $(H_0, \Omega_m, r_d) = (67.36, 0.315, 147.09)$.

Nevertheless, armed with a new PD methodology, we are in a position to revisit the earlier result and see if we can recover the 2σ tension with Planck. Since [30] made use of older BAO data, here we replace QSO and Lyman- α BAO with the latest eBOSS results [73–75]. Moreover, we work directly with the D_H/r_d constraints and do not invert them. This entails assuming a value for the radius of the sound horizon, which we take to be the Planck value, $r_d = 147.09 \pm 0.26$ Mpc [1]. In addition, we reinstate the prior $\Omega_m h^2 = 0.1430 \pm 0.0011$, so that the only difference with [30] is simply to update OHD BAO to the latest constraints. We stress that the priors we introduce are consistent with the Planck cosmology, so *they cannot be driving any disagreement*. Moreover, the $\Omega_m h^2$ prior restricts one to a curve in the (H_0, Ω_m) , but it cannot dictate where one is on the curve, this is done by the remaining 3 CC and 3 BAO data points.

We again marginalise over the free parameters (H_0, Ω_m, r_d) with MCMC. In Fig. 6 we present the posteriors. While r_d is Gaussian and peaked on our Planck prior, as expected, the Ω_m posterior is peaked at $\Omega_m \sim 0.6$ and the fact that the fall off in the distribution is

⁹This prior essentially prevents high redshift CC data from tracking a non-evolving $H(z)$.

gradual beyond the peak leads to a pile up of configurations in the top left corner of the (H_0, Ω_m) -plane. This fall off continues beyond $\Omega_m = 1$ and if the prior is relaxed, the H_0 peak shifts to smaller values. So, once again all the hallmarks of projection effects are present. That being said, given the sharp fall off in the Ω_m distribution to smaller Ω_m values, some tension appears to be evident with the Planck values (dashed lines).

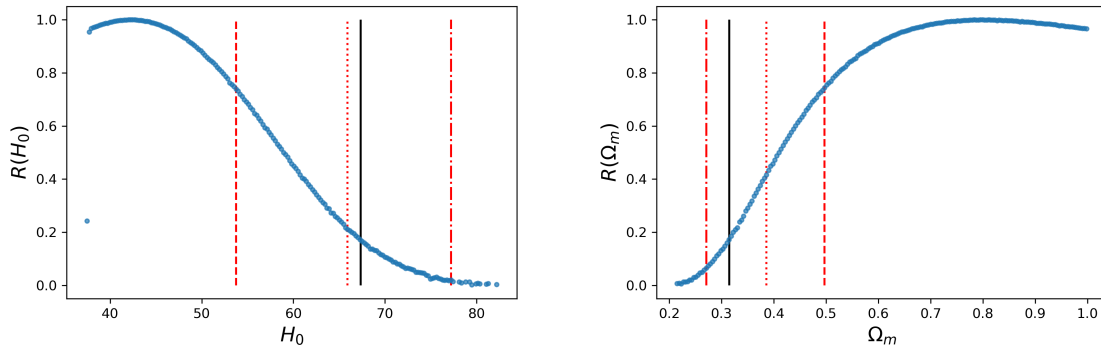


Figure 7. $R(H_0)$ and $R(\Omega_m)$ distributions for CC and BAO OHD with redshift $z > 1.45$ subject to Planck priors on $\Omega_m h^2$ and r_d . The dashed, dotted and dashed-dotted lines denote 1σ , 2σ and 3σ confidence intervals and the solid black line is the Planck best fit value.

We now run the MCMC chain through our PD methodology. From Fig. 7, we can see that the $R(H_0)$ and $R(\Omega_m)$ distributions prefer smaller values of H_0 and larger values of Ω_m . The peak of the distributions occurs at $H_0 = 42.40$ km/s/Mpc and $\Omega_m = 0.795$. The lone dot in the $R(H_0)$ distribution at low values of H_0 tells us that the distribution falls off sharply below $H_0 = 40$ km/s/Mpc. Note, since we employed generous uniform priors $H_0 \in [0, 200]$, the priors are not impacting the $R(H_0)$ distribution, so it is expected that the distribution falls off to zero on both sides. In contrast, the $R(\Omega_m)$ distribution is one-sided and fails to fall off in the direction of larger values within the uniform priors $\Omega_m \in [0, 1]$. The tension with Planck falls between 2σ and 3σ . By integrating the PDF as far as the black lines corresponding to the Planck values in Fig. 7, we estimate that the Planck H_0 is located at 2.1σ from the peak, while the Planck Ω_m value is 2.5σ from the peak.

The main take-away from this section is that OHD data comprising CC and BAO data points beyond $z = 1.45$ is inconsistent with the Planck cosmology at in excess of 2σ . We have employed Planck priors to arrive at this result, but these priors cannot drive the disagreement. Moreover, independent analysis based on least squares fitting and mock simulations presented in [30] also points to a 2σ tension, albeit with less up-to-date high redshift BAO data. In summary, different methodologies agree on a 2σ discrepancy with Planck, which is robust to interchanging older and newer BAO data.

5 Concluding remarks

A χ^2 likelihood is a metric or measure of how well a model fits data. The point in model parameter space that fits the data the best possesses the lowest χ^2 . Once one has identified this point, the problem remains to establish 1σ , 2σ , etc, confidence intervals in parameter space. In cosmology and astrophysics, MCMC is the prevailing technique for estimating confidence intervals. Its great advantage is that it allows one to i) globally sample the parameter space

and ii) arrive at posteriors that serve as an estimate of the errors even with non-Gaussian distributions. In contrast, if one minimises the χ^2 by gradient descent, there is always a risk that one ends up in a local minimum, i. e. the global minimum is missed, while error estimation through Fisher matrix assumes any distribution is Gaussian. The appeal of MCMC marginalisation is that it is widely applicable. However, the point of this paper is that limitations exist, even in the simplest model.

Indeed, what happens when the MCMC posterior no longer tracks points in parameter space that fit the data better? Traditionally, volume effects are seen as the preserve of higher-dimensional models, e. g. [56–58], but projection effects also occur in the minimal Λ CDM model when one fits the model to data binned by redshift in the late Universe [48]. As explained in [48], this “projection effect” is driven by OHD, $H(z_i)$, and angular diameter or luminosity distance data, $D_A(z_i)$ or $D_L(z_i)$, respectively only constraining the combinations $\Omega_m h^2$ and $(1 - \Omega_m)h^2$ well, with high redshift data $z_i \gg 0$. In practice, this restricts MCMC configurations to constant $\Omega_m h^2$ and constant $(1 - \Omega_m)h^2$ curves in the (H_0, Ω_m) plane, and as the curves stretch due to DE or matter being less well constrained in high redshift bins, projection effects lead to shifts in the peaks of MCMC posteriors and the emergence of non-Gaussian tails [48]. We stress that one sees the same effect in PDFs of best fit (H_0, Ω_m) parameters in a large number of mock data realisations [48], so the problem is more general than MCMC; there is an inherent bias in the Λ CDM model when one fits it to redshift binned $H(z)$ or $D_A(z)$ or $D_L(z)$ data. Within MCMC, one sees this effect in the errors, but also in the drift of the parameters corresponding to the χ^2 minimum outside of the 1σ confidence intervals. Highlighting this (expected) bias in MCMC using OHD is the opening salvo (result) of this paper.

Why should one care? This is evidently only a problem if one bins data and confronts the Λ CDM model. First, note that some data sets are inherently binned. For example, effective redshifts are assigned to CC and BAO analysed in a given redshift bin, while each strongly lensed system constitutes its own bin. Working with binned data is unavoidable. Secondly, Λ CDM tensions point to a problem with the Λ CDM model once the tensions become widespread and persistent. As explained in [22], if the minimal Λ CDM model is too simple, one expects redshift evolution of Λ CDM cosmological parameters as it is confronted to redshift binned data. Hints of these trends are now evident in H_0 [24, 25, 28–35], Ω_m [29–31, 36–43, 45, 47] and S_8/σ_8 [49–52] (also [54, 55]) across a host of different observables. This evolution is an expected hallmark of model breakdown, which must happen at some redshift if systematics are not universally at play.

The main problem with redshift dependent Λ CDM cosmological parameters¹⁰ is one needs to assign a statistical significance to any trend. At a purely practical level, this entails constructing bins centered on different redshifts and identifying discrepancies in Λ CDM parameters between bins, *ideally in the same observable*, so that the potential systematics are under greatest control. As demonstrated both mathematically and observationally with the CC data in section 2, MCMC marginalisation leads to biased inferences when one bins the data. In this paper we have resorted to profile distributions [57] to overcome this bias

¹⁰There is a separate interpretation problem as the cosmology literature works with parameters “defined today”. In more mathematical language, this is simply the statement that one solves an ordinary differential equation (ODE), namely the Friedmann equation or equivalent, by specifying an integration constant, e.g. $H_0 = H(z=0)$ or $\rho_m(z=0) = \rho_{m0} = H_0^2 \Omega_m$. However, this is a mathematical statement and it still needs to be confirmed observationally that H_0 or ρ_{m0} are *bona fide* constants. This cannot be *a priori* assumed, because it is mathematical prediction of the model. If the model is correct, a constant H_0 and Ω_m will be supported by the data. See [22] for further discussion.

and have applied the technique to a setting where Λ CDM distributions are expected to be non-Gaussian for the reasons outlined above and in section 2. This new technique, provides a complementary perspective that confirms the least square fits of observed and mock data presented in [29–31], where evidence for redshift evolution in H_0 and Ω_m was presented. Regardless of the methodology, the objective is to drill down on the prevailing *assumption* that cosmological parameters are constants. *In the era of tensions in cosmology, nothing can be assumed, especially noting that the tensions are in essence showing an example of evolution of these parameters with redshift.*

More concretely, in this paper with both mock simulations and profile distributions we have shown that high redshift CC data has a preference for a non-evolving $H(z)$ over Planck- Λ CDM at approximately $\sim 2\sigma$. This trend, which constitutes the second result of the paper, is unquestionable, as it is visible in the data. Note, we have not propagated systematic uncertainties, so the significance will be less when these are properly propagate. Nevertheless, low and high redshift CC data currently have a preference for different Λ CDM cosmological parameters. This is important because if the CC program is claiming an 8% constraint on the Hubble constant, $H_0 = 66.7 \pm 5.5$ km/s/Mpc [70], it is imperative that *all subsets of the data are consistent with this result*. If they are not, then we are staring at either systematics or model breakdown. Admittedly, demanding self-consistency of subsets of a data set confronted to a model is a high bar, but it is important that data sets result in overlapping constraints on Λ CDM parameters, otherwise this makes cosmological inferences moot. Note, the Λ CDM model is largely only well tested in the DE dominated regime $z \lesssim 1$ and at very high redshifts $z \sim 1100$, which leaves a wide expanse of redshifts to be explored in order to confirm or refute the model. Given the existing Λ CDM tensions [15, 16], and the hints of evolution in H_0 , Ω_m and S_8 across assorted probes in the late Universe $z \lesssim 5$, it would be surprising if all discrepancies could be explained away by systematics.¹¹

As an aside, it is intriguing that CC data has a preference for larger best fit values of H_0 and smaller best fit values of Ω_m beyond $z_{\min} = 0.7$, as this is traditionally the transition redshift between decelerated and accelerated expansion. Moreover, at higher redshifts $z \sim 2.3$, there is not only a longstanding anomaly in Lyman- α BAO [75], but QSOs also show a preference for a lower luminosity distance, $D_L(z)$, relative to Planck- Λ CDM [36, 37]. Translated into Λ CDM parameters, this corresponds to conversely larger Ω_m values, e. g. [39–43], and consequently smaller H_0 values. Thus, the emerging probes CC and QSOs [77] do not appear to be in sync on high redshift Λ CDM inferences. Nevertheless, neither may be inconsistent with the anomaly in Lyman- α BAO. Relative to Planck- Λ CDM, Lyman- α BAO prefers *smaller* values of $D_M(z) := c \int_0^z 1/H(z') dz$ and *smaller* values of $H(z)$ (larger values of $D_H(z) := c/H(z)$).¹² If CC data prefer less evolution in $H(z)$ in the matter-dominated regime, then this is consistent with the preference for a smaller $H(z)$ from Lyman- α BAO. Furthermore, QSO data prefers smaller luminosity distances $D_L(z)$ relative to Planck, which

¹¹We are open to the possibility, we just consider it a bad bet at the moment. The odds can of course change as observations improve.

¹²In this statement we assumed the Planck value $r_d \sim 147$ Mpc [1] If we reinstate the radius of the sound horizon in these expressions, one recognises that changing the sound horizon, as advocated by early Universe resolutions to Hubble tension, cannot consistently address the Lyman- α BAO anomaly. In general, even for the Planck- Λ CDM sound horizon, one cannot get both a smaller $D_M(z)$ and smaller $H(z)$ from a strictly increasing function, such as the Λ CDM $H(z)$. As a result, deviations from the Planck- Λ CDM model that address this anomaly are expected to lead to wiggles in $H(z)$ [79], which are unsurprisingly seen in data reconstructions [80–82]. Finally, evolution in H_0, Ω_m discussed here cannot be explained or accommodated by early resolutions to Hubble tension relying on a change in the r_d at very high z .

are consistent with the smaller $D_M(z) \propto D_L(z)$ values preferred by Lyman- α BAO. Thus, even if CC and QSOs appear to be showing diverging behaviour in the cosmological parameters (H_0, Ω_m) , this may still turn out to be consistent with Lyman- α BAO. We await future DESI [78] data releases to ascertain if the non-evolving $H(z)$ trend in high redshift CC data is physical or not.

Finally, we come to our third and main result outlined in section 4. We have revisited a $\sim 2\sigma$ tension between high redshift CC and BAO data reported in [30], where the significance was estimated through mock simulations. Here, we have upgraded the BAO data to the latest constraints and again recover a $> 2\sigma$ discrepancy in (H_0, Ω_m) with different methodology. This provides a consistency check that there is evolution in OHD between low and high redshifts in the late Universe. Note, this evolution runs contrary to the non-evolving $H(z)$ seen in high redshift CC data because it assumes Planck has accurately constrained the high redshift behaviour of the Hubble parameter in (2.1). Nevertheless, both with and without a Planck prior on $\Omega_m h^2$, evolution at $\gtrsim 2\sigma$ is evident in OHD data. It should be stressed that evolution is evident in PDFs of best fit Λ CDM parameters fitted to a large number of Planck- Λ CDM mocks [48], so evolution in observed data can be expected. It is imperative to revisit the remaining observations in [30, 31] in order to confirm the significance of $\sim 2\sigma$ hints of evolution found separately in Type Ia SN and QSO data sets.

Acknowledgments

We would like to thank Adrià Gómez-Valent for discussions and comments on the draft. We thank Gabriela Marques, Mike Hudson and Matteo Viel for related discussions on late Universe evolution in S_8 . EÓC thanks Yonsei University and Asia Pacific Center for Theoretical Physics for hospitality. This article/publication is based upon work from COST Action CA21136 – “Addressing observational tensions in cosmology with systematics and fundamental physics (CosmoVerse)”, supported by COST (European Cooperation in Science and Technology). SP and MMSHJ acknowledge SarAmadan grant No. ISEF/M/401332. MMSHJ thanks the support from ICTP associates office (under Senior Associate program) and ICTP HECAP section for hospitality.

A Fisher Matrix

Consider the χ^2 (2.2). Defining $H_{\text{model}}(z) = H_0 \sqrt{1 - \Omega_m + \Omega_m(1+z)^3}$ and Q_i as in (2.3), we can now work out the derivatives

$$\begin{aligned}
\partial_{H_0} Q_i &= -\sqrt{1 - \Omega_m + \Omega_m(1+z_i)^3}, \\
\partial_{\Omega_m} Q_i &= -\frac{1}{2} H_0 (z_i^3 + 3z_i^2 + 3z_i) / \sqrt{1 - \Omega_m + \Omega_m(1+z_i)^3}, \\
\partial_{H_0}^2 Q_i &= 0, \\
\partial_{H_0} \partial_{\Omega_m} Q_i &= -\frac{1}{2} (z_i^3 + 3z_i^2 + 3z_i) / \sqrt{1 - \Omega_m + \Omega_m(1+z_i)^3}, \\
\partial_{\Omega_m}^2 Q_i &= \frac{1}{4} H_0 (z_i^3 + 3z_i^2 + 3z_i)^2 / (1 - \Omega_m + \Omega_m(1+z_i)^3)^{\frac{3}{2}}.
\end{aligned}
\tag{A.1}$$

We can then define the Fisher matrix

$$F_{ij} = \frac{1}{2} \frac{\partial^2 \chi^2(H_0, \Omega_m)}{\partial p_i \partial p_j}
\tag{A.2}$$

where $p_i \in \{H_0, \Omega_m\}$. Note that the Fisher matrix is evaluated on the best fit parameters. The result is a 2×2 matrix, which one inverts and the estimated errors are the square root of the diagonal entries.

References

- [1] N. Aghanim *et al.* [Planck], “Planck 2018 results. VI. Cosmological parameters,” *Astron. Astrophys.* **641** (2020), A6
- [2] A. G. Riess *et al.* [Supernova Search Team], “Observational evidence from supernovae for an accelerating universe and a cosmological constant,” *Astron. J.* **116** (1998), 1009-1038
- [3] S. Perlmutter *et al.* [Supernova Cosmology Project], “Measurements of Ω and Λ from 42 high redshift supernovae,” *Astrophys. J.* **517** (1999), 565-586
- [4] D. J. Eisenstein *et al.* [SDSS], “Detection of the Baryon Acoustic Peak in the Large-Scale Correlation Function of SDSS Luminous Red Galaxies,” *Astrophys. J.* **633** (2005), 560-574
- [5] A. G. Riess, W. Yuan, L. M. Macri, D. Scolnic, D. Brout, S. Casertano, D. O. Jones, Y. Murakami, L. Breuval and T. G. Brink, *et al.* “A Comprehensive Measurement of the Local Value of the Hubble Constant with 1 km s⁻¹ Mpc⁻¹ Uncertainty from the Hubble Space Telescope and the SH0ES Team,” *Astrophys. J. Lett.* **934** (2022) no.1, L7
- [6] W. L. Freedman, “Measurements of the Hubble Constant: Tensions in Perspective,” *Astrophys. J.* **919** (2021) no.1, 16
- [7] D. W. Pesce, J. A. Braatz, M. J. Reid, A. G. Riess, D. Scolnic, J. J. Condon, F. Gao, C. Henkel, C. M. V. Impellizzeri and C. Y. Kuo, *et al.* *Astrophys. J. Lett.* **891** (2020) no.1, L1
- [8] J. P. Blakeslee, J. B. Jensen, C. P. Ma, P. A. Milne and J. E. Greene, *Astrophys. J.* **911** (2021) no.1, 65
- [9] E. Kourkchi, R. B. Tully, G. S. Anand, H. M. Courtois, A. Dupuy, J. D. Neill, L. Rizzi and M. Seibert, *Astrophys. J.* **896** (2020) no.1, 3
- [10] C. Hikage *et al.* [HSC], “Cosmology from cosmic shear power spectra with Subaru Hyper Suprime-Cam first-year data,” *Publ. Astron. Soc. Jap.* **71**, 43 (2019).
- [11] M. Asgari *et al.* [KiDS], “KiDS-1000 Cosmology: Cosmic shear constraints and comparison between two point statistics,” *Astron. Astrophys.* **645** (2021), A104
- [12] T. M. C. Abbott *et al.* [DES], “Dark Energy Survey Year 3 results: Cosmological constraints from galaxy clustering and weak lensing,” *Phys. Rev. D* **105** (2022) no.2, 023520
- [13] S. S. Boruah, M. J. Hudson and G. Lavaux, “Cosmic flows in the nearby Universe: new peculiar velocities from SNe and cosmological constraints,” *Mon. Not. Roy. Astron. Soc.* **498** (2020) no.2, 2703-2718
- [14] K. Said, M. Colless, C. Magoulas, J. R. Lucey and M. J. Hudson, “Joint analysis of 6dFGS and SDSS peculiar velocities for the growth rate of cosmic structure and tests of gravity,” *Mon. Not. Roy. Astron. Soc.* **497** (2020) no.1, 1275-1293
- [15] L. Perivolaropoulos and F. Skara, “Challenges for Λ CDM: An update,” *New Astron. Rev.* **95**, 101659 (2022).
- [16] E. Abdalla, G. Franco Abellán, A. Aboubrahim, A. Agnello, O. Akarsu, Y. Akrami, G. Alestas, D. Aloni, L. Amendola and L. A. Anchordoqui, *et al.* “Cosmology intertwined: A review of the particle physics, astrophysics, and cosmology associated with the cosmological tensions and anomalies,” *JHEAp* **34**, 49 (2022).
- [17] M. M. Phillips, “The absolute magnitudes of Type IA supernovae,” *Astrophys. J. Lett.* **413** (1993), L105-L108

- [18] M. Rigault *et al.* [Nearby Supernova Factory], “Strong Dependence of Type Ia Supernova Standardization on the Local Specific Star Formation Rate,” *Astron. Astrophys.* **644** (2020), A176
- [19] Y. Kang, Y. W. Lee, Y. L. Kim, C. Chung and C. H. Ree, “Early-type Host Galaxies of Type Ia Supernovae. II. Evidence for Luminosity Evolution in Supernova Cosmology,” *Astrophys. J.* **889** (2020) no.1, 8
- [20] D. Brout and D. Scolnic, “It’s Dust: Solving the Mysteries of the Intrinsic Scatter and Host-galaxy Dependence of Standardized Type Ia Supernova Brightnesses,” *Astrophys. J.* **909** (2021) no.1, 26
- [21] Y. W. Lee, C. Chung, P. Demarque, S. Park, J. Son and Y. Kang, “Evidence for strong progenitor age dependence of type Ia supernova luminosity standardization process,” *Mon. Not. Roy. Astron. Soc.* **517** (2022) no.2, 2697-2708
- [22] C. Krishnan, E. Ó Colgáin, M. M. Sheikh-Jabbari and T. Yang, “Running Hubble Tension and a H0 Diagnostic,” *Phys. Rev. D* **103** (2021) no.10, 103509
- [23] C. Krishnan and R. Mondol, “ H_0 as a Universal FLRW Diagnostic,” [arXiv:2201.13384 [astro-ph.CO]].
- [24] K. C. Wong, S. H. Suyu, G. C. F. Chen, C. E. Rusu, M. Millon, D. Sluse, V. Bonvin, C. D. Fassnacht, S. Taubenberger and M. W. Auger, *et al.* “H0LiCOW – XIII. A 2.4 per cent measurement of H0 from lensed quasars: 5.3σ tension between early- and late-Universe probes,” *Mon. Not. Roy. Astron. Soc.* **498** (2020) no.1, 1420-1439
- [25] M. Millon, A. Galan, F. Courbin, T. Treu, S. H. Suyu, X. Ding, S. Birrer, G. C. F. Chen, A. J. Shajib and D. Sluse, *et al.* “TDCOSMO. I. An exploration of systematic uncertainties in the inference of H_0 from time-delay cosmography,” *Astron. Astrophys.* **639** (2020), A101
- [26] D. Sluse, J. Surdej, J. F. Claeskens, D. Hutsemekers, C. Jean, F. Courbin, T. Nakos, M. Billeres and S. V. Khmil, “A Quadruply imaged quasar with an optical Einstein ring candidate: 1RXS J113155.4-123155,” *Astron. Astrophys.* **406** (2003), L43-L46
- [27] A. J. Shajib, P. Mozumdar, G. C. F. Chen, T. Treu, M. Cappellari, S. Knabel, S. H. Suyu, V. N. Bennert, J. A. Frieman and D. Sluse, *et al.* “TDCOSMO. XIII. Improved Hubble constant measurement from lensing time delays using spatially resolved stellar kinematics of the lens galaxy,” *Astron. Astrophys.* **673** (2023), A9
- [28] M. G. Dainotti, B. De Simone, T. Schiavone, G. Montani, E. Rinaldi and G. Lambiase, “On the Hubble constant tension in the SNe Ia Pantheon sample,” *Astrophys. J.* **912**, 150 (2021).
- [29] E. Ó Colgáin, M. M. Sheikh-Jabbari, R. Solomon, G. Bargiacchi, S. Capozziello, M. G. Dainotti and D. Stojkovic, “Revealing intrinsic flat Λ CDM biases with standardizable candles,” *Phys. Rev. D* **106**, L041301 (2022).
- [30] E. Ó Colgáin, M. M. Sheikh-Jabbari, R. Solomon, M. G. Dainotti and D. Stojkovic, “Putting Flat Λ CDM In The (Redshift) Bin,” [arXiv:2206.11447 [astro-ph.CO]].
- [31] M. Malekjani, R. M. Conville, E. Ó. Colgáin, S. Pourojaghi and M. M. Sheikh-Jabbari, “Negative Dark Energy Density from High Redshift Pantheon+ Supernovae,” [arXiv:2301.12725 [astro-ph.CO]].
- [32] J. P. Hu and F. Y. Wang, “Revealing the late-time transition of H0: relieve the Hubble crisis,” *Mon. Not. Roy. Astron. Soc.* **517**, 576 (2022).
- [33] X. D. Jia, J. P. Hu and F. Y. Wang, “Evidence of a decreasing trend for the Hubble constant,” *Astron. Astrophys.* **674** (2023), A45
- [34] C. Krishnan, E. Ó Colgáin, Ruchika, A. A. Sen, M. M. Sheikh-Jabbari and T. Yang, “Is there an early Universe solution to Hubble tension?,” *Phys. Rev. D* **102** (2020) no.10, 103525

- [35] M. G. Dainotti, B. De Simone, T. Schiavone, G. Montani, E. Rinaldi, G. Lambiase, M. Bogdan and S. Ugale, “On the Evolution of the Hubble Constant with the SNe Ia Pantheon Sample and Baryon Acoustic Oscillations: A Feasibility Study for GRB-Cosmology in 2030,” *Galaxies* **10**, 24 (2022).
- [36] G. Risaliti and E. Lusso, “A Hubble Diagram for Quasars,” *Astrophys. J.* **815** (2015), 33
- [37] G. Risaliti and E. Lusso, “Cosmological constraints from the Hubble diagram of quasars at high redshifts,” *Nature Astron.* **3**, 272 (2019).
- [38] E. Lusso, G. Risaliti, E. Nardini, G. Bargiacchi, M. Benetti, S. Bisogni, S. Capozziello, F. Civano, L. Eggleston and M. Elvis, *et al.* “Quasars as standard candles III. Validation of a new sample for cosmological studies,” *Astron. Astrophys.* **642**, A150 (2020).
- [39] T. Yang, A. Banerjee and E. Ó Colgáin, “Cosmography and flat Λ CDM tensions at high redshift,” *Phys. Rev. D* **102**, 123532 (2020).
- [40] N. Khadka and B. Ratra, “Using quasar X-ray and UV flux measurements to constrain cosmological model parameters,” *Mon. Not. Roy. Astron. Soc.* **497**, 263 (2020).
- [41] N. Khadka and B. Ratra, “Determining the range of validity of quasar X-ray and UV flux measurements for constraining cosmological model parameters,” *Mon. Not. Roy. Astron. Soc.* **502**, 6140 (2021).
- [42] N. Khadka and B. Ratra, “Do quasar X-ray and UV flux measurements provide a useful test of cosmological models?,” *Mon. Not. Roy. Astron. Soc.* **510**, 2753 (2022).
- [43] S. Pourojaghi, N. F. Zabihi and M. Malekjani, “Can high-redshift Hubble diagrams rule out the standard model of cosmology in the context of cosmography?,” *Phys. Rev. D* **106**, 123523 (2022).
- [44] M. Zajaček, B. Czerny, N. Khadka, R. Prince, S. Panda, M. L. Martínez-Aldama and B. Ratra, “Extinction biases quasar luminosity distances determined from quasar UV and X-ray flux measurements,” [arXiv:2305.08179 [astro-ph.GA]].
- [45] E. Pastén and V. H. Cárdenas, “Testing Λ CDM cosmology in a binned universe: Anomalies in the deceleration parameter,” *Phys. Dark Univ.* **40** (2023), 101224
- [46] J. Wagner, “Casting the H_0 tension as a fitting problem of cosmologies,” [arXiv:2203.11219 [astro-ph.CO]].
- [47] Z. Sakr, “One matter density discrepancy to alleviate them all or further trouble for Λ CDM model,” [arXiv:2305.02846 [astro-ph.CO]].
- [48] E. Ó Colgáin, M. M. Sheikh-Jabbari and R. Solomon, “High redshift Λ CDM cosmology: To bin or not to bin?,” *Phys. Dark Univ.* **40** (2023), 101216 [arXiv:2211.02129 [astro-ph.CO]].
- [49] M. Esposito, V. Iršič, M. Costanzi, S. Borgani, A. Saro and M. Viel, “Weighing cosmic structures with clusters of galaxies and the intergalactic medium,” *Mon. Not. Roy. Astron. Soc.* **515**, 857 (2022). [arXiv:2202.00974 [astro-ph.CO]].
- [50] S. A. Adil, Ö. Akarsu, M. Malekjani, E. Ó Colgáin, S. Pourojaghi, A. A. Sen and M. M. Sheikh-Jabbari, “ S_8 increases with effective redshift in Λ CDM cosmology,” [arXiv:2303.06928 [astro-ph.CO]].
- [51] F. J. Qu *et al.* [ACT], “The Atacama Cosmology Telescope: A Measurement of the DR6 CMB Lensing Power Spectrum and its Implications for Structure Growth,” [arXiv:2304.05202 [astro-ph.CO]].
- [52] M. S. Madhavacheril *et al.* [ACT], “The Atacama Cosmology Telescope: DR6 Gravitational Lensing Map and Cosmological Parameters,” [arXiv:2304.05203 [astro-ph.CO]].
- [53] G. A. Marques *et al.* [ACT and DES], “Cosmological constraints from the tomography of DES-Y3 galaxies with CMB lensing from ACT DR4,” [arXiv:2306.17268 [astro-ph.CO]].

- [54] H. Miyatake, Y. Harikane, M. Ouchi, Y. Ono, N. Yamamoto, A. J. Nishizawa, N. Bahcall, S. Miyazaki and A. A. Plazas Malagón, “First Identification of a CMB Lensing Signal Produced by 1.5 Million Galaxies at $z \sim 4$: Constraints on Matter Density Fluctuations at High Redshift,” *Phys. Rev. Lett.* **129** (2022) no.6, 061301 [arXiv:2103.15862 [astro-ph.CO]].
- [55] D. Alonso, G. Fabbian, K. Storey-Fisher, A. C. Eilers, C. García-García, D. W. Hogg and H. W. Rix, “Constraining cosmology with the Gaia-unWISE Quasar Catalog and CMB lensing: structure growth,” [arXiv:2306.17748 [astro-ph.CO]].
- [56] L. Herold, E. G. M. Ferreira and E. Komatsu, “New Constraint on Early Dark Energy from Planck and BOSS Data Using the Profile Likelihood,” *Astrophys. J. Lett.* **929** (2022) no.1, L16
- [57] A. Gómez-Valent, “Fast test to assess the impact of marginalization in Monte Carlo analyses and its application to cosmology,” *Phys. Rev. D* **106** (2022) no.6, 063506
- [58] M. Meiers, L. Knox and N. Schöneberg, “Exploration of the Pre-recombination Universe with a High-Dimensional Model of an Additional Dark Fluid,” [arXiv:2307.09522 [astro-ph.CO]].
- [59] V. Poulin, T. L. Smith, T. Karwal and M. Kamionkowski, “Early Dark Energy Can Resolve The Hubble Tension,” *Phys. Rev. Lett.* **122** (2019) no.22, 221301
- [60] F. Niedermann and M. S. Sloth, “New early dark energy,” *Phys. Rev. D* **103** (2021) no.4, L041303 [arXiv:1910.10739 [astro-ph.CO]].
- [61] R. Jimenez and A. Loeb, “Constraining cosmological parameters based on relative galaxy ages,” *Astrophys. J.* **573** (2002), 37-42
- [62] D. Stern, R. Jimenez, L. Verde, M. Kamionkowski and S. A. Stanford, “Cosmic Chronometers: Constraining the Equation of State of Dark Energy. I: $H(z)$ Measurements,” *JCAP* **02** (2010), 008
- [63] M. Moresco, A. Cimatti, R. Jimenez, L. Pozzetti, G. Zamorani, M. Bolzonella, J. Dunlop, F. Lamareille, M. Mignoli and H. Pearce, *et al.* “Improved constraints on the expansion rate of the Universe up to $z \sim 1.1$ from the spectroscopic evolution of cosmic chronometers,” *JCAP* **08** (2012), 006
- [64] C. Zhang, H. Zhang, S. Yuan, T. J. Zhang and Y. C. Sun, “Four new observational $H(z)$ data from luminous red galaxies in the Sloan Digital Sky Survey data release seven,” *Res. Astron. Astrophys.* **14** (2014) no.10, 1221-1233
- [65] M. Moresco, L. Pozzetti, A. Cimatti, R. Jimenez, C. Maraston, L. Verde, D. Thomas, A. Citro, R. Tojeiro and D. Wilkinson, “A 6% measurement of the Hubble parameter at $z \sim 0.45$: direct evidence of the epoch of cosmic re-acceleration,” *JCAP* **05** (2016), 014
- [66] A. L. Ratsimbazafy, S. I. Loubser, S. M. Crawford, C. M. Cress, B. A. Bassett, R. C. Nichol and P. Väisänen, “Age-dating Luminous Red Galaxies observed with the Southern African Large Telescope,” *Mon. Not. Roy. Astron. Soc.* **467** (2017) no.3, 3239-3254
- [67] N. Borghi, M. Moresco and A. Cimatti, “Toward a Better Understanding of Cosmic Chronometers: A New Measurement of $H(z)$ at $z \sim 0.7$,” *Astrophys. J. Lett.* **928** (2022) no.1, L4
- [68] K. Jiao, N. Borghi, M. Moresco and T. J. Zhang, “New Observational $H(z)$ Data from Full-spectrum Fitting of Cosmic Chronometers in the LEGA-C Survey,” *Astrophys. J. Suppl.* **265** (2023) no.2, 48
- [69] E. Tomasetti, M. Moresco, N. Borghi, K. Jiao, A. Cimatti, L. Pozzetti, A. C. Carnall, R. J. McLure and L. Pentericci, “A new measurement of the expansion history of the Universe at $z=1.26$ with cosmic chronometers in VANDELS,” [arXiv:2305.16387 [astro-ph.CO]].
- [70] M. Moresco, “Addressing the Hubble tension with cosmic chronometers,” [arXiv:2307.09501 [astro-ph.CO]].

- [71] M. Moresco, R. Jimenez, L. Verde, A. Cimatti and L. Pozzetti, “Setting the Stage for Cosmic Chronometers. II. Impact of Stellar Population Synthesis Models Systematics and Full Covariance Matrix,” *Astrophys. J.* **898** (2020) no.1, 82 [arXiv:2003.07362 [astro-ph.GA]].
- [72] D. Foreman-Mackey, D. W. Hogg, D. Lang and J. Goodman, “emcee: The MCMC Hammer,” *Publ. Astron. Soc. Pac.* **125** (2013), 306-312
- [73] J. Hou, A. G. Sánchez, A. J. Ross, A. Smith, R. Neveux, J. Bautista, E. Burtin, C. Zhao, R. Scoccimarro and K. S. Dawson, *et al.* “The Completed SDSS-IV extended Baryon Oscillation Spectroscopic Survey: BAO and RSD measurements from anisotropic clustering analysis of the Quasar Sample in configuration space between redshift 0.8 and 2.2,” *Mon. Not. Roy. Astron. Soc.* **500** (2020) no.1, 1201-1221
- [74] R. Neveux, E. Burtin, A. de Mattia, A. Smith, A. J. Ross, J. Hou, J. Bautista, J. Brinkmann, C. H. Chuang and K. S. Dawson, *et al.* “The completed SDSS-IV extended Baryon Oscillation Spectroscopic Survey: BAO and RSD measurements from the anisotropic power spectrum of the quasar sample between redshift 0.8 and 2.2,” *Mon. Not. Roy. Astron. Soc.* **499** (2020) no.1, 210-229
- [75] H. du Mas des Bourboux, J. Rich, A. Font-Ribera, V. de Sainte Agathe, J. Farr, T. Etourneau, J. M. Le Goff, A. Cuceu, C. Balland and J. E. Bautista, *et al.* “The Completed SDSS-IV Extended Baryon Oscillation Spectroscopic Survey: Baryon Acoustic Oscillations with Ly α Forests,” *Astrophys. J.* **901** (2020) no.2, 153
- [76] R. Trotta, “Bayesian Methods in Cosmology,” [arXiv:1701.01467 [astro-ph.CO]].
- [77] M. Moresco, L. Amati, L. Amendola, S. Birrer, J. P. Blakeslee, M. Cantiello, A. Cimatti, J. Darling, M. Della Valle and M. Fishbach, *et al.* “Unveiling the Universe with emerging cosmological probes,” *Living Rev. Rel.* **25** (2022) no.1, 6
- [78] G. Adame *et al.* [DESI], “The Early Data Release of the Dark Energy Spectroscopic Instrument,” [arXiv:2306.06308 [astro-ph.CO]].
- [79] O. Akarsu, E. Ó Colgáin, E. Özulker, S. Thakur and L. Yin, “Inevitable manifestation of wiggles in the expansion of the late Universe,” *Phys. Rev. D* **107** (2023) no.12, 123526
- [80] G. B. Zhao, M. Raveri, L. Pogosian, Y. Wang, R. G. Crittenden, W. J. Handley, W. J. Percival, F. Beutler, J. Brinkmann and C. H. Chuang, *et al.* “Dynamical dark energy in light of the latest observations,” *Nature Astron.* **1** (2017) no.9, 627-632
- [81] Y. Wang, L. Pogosian, G. B. Zhao and A. Zucca, “Evolution of dark energy reconstructed from the latest observations,” *Astrophys. J. Lett.* **869** (2018), L8
- [82] L. A. Escamilla and J. A. Vazquez, “Model selection applied to reconstructions of the Dark Energy,” *Eur. Phys. J. C* **83** (2023) no.3, 251